Peyvasteh Motahareh (Orcid ID: 0000-0001-7543-8320)

Full Article

Evolution of raw meat polarization-based properties by means of Mueller matrix imaging

Motahareh Peyvasteh[1*] | Alexey Popov[2] | Alexander Bykov[1] | Angelo Pierangelo[3] | Tatiana Novikova[3] | Igor Meglinski[1,4,5,6,7*]

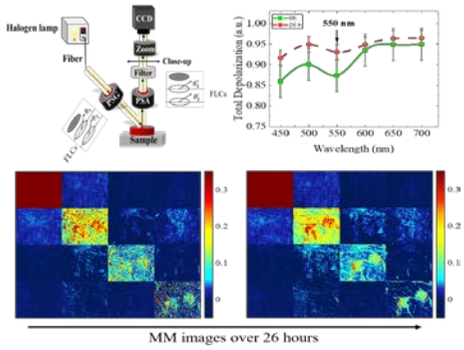

1 Opto-Electronic and Measurement Techniques research unit, University of Oulu, Oulu, Finland

2 VTT Technical Research Centre of Finland, Oulu, Finland

3 Laboratory of Physics of Interfaces and Thin Films, École Polytechnique, Palaiseau, France

4 Institute of Engineering Physics for Biomedicine (PhysBio), National Research Nuclear University "MEPhI", Moscow, Russia

5 Interdisciplinary Laboratory of Biophotonics, National Research Tomsk State University, Tomsk, Russia

6 Department of Histology, Cytology and Embryology, Institute of Clinical Medicine N.V. Sklifosovsky, I.M. Sechenov First Moscow State Medical University, Moscow, Russia

7 College of Engineering and Physical Sciences, Aston University, Birmingham, United Kingdom

*** Correspondence:**

Motahareh Peyvasteh, Opto-Electronic and Measurement Techniques research unit, University of Oulu, P.O. Box 4500, 90014 Oulu, Finland

E-mail: motahareh.peyvasteh@oulu.fi

Igor Meglinski, College of Engineering and Physical Sciences, Aston University, B4 7ET Birmingham, United Kingdom

E-mail: i.meglinski@aston.ac.uk

This article has been accepted for publication and undergone full peer review but has not been through the copyediting, typesetting, pagination and proofreading process which may lead to differences between this version and the Version of Record. Please cite this article as doi: 10.1002/jbio.202000376

The possibilities of using Mueller matrix (MM) imaging polarimetry to assess meat quality have not yet been sufficiently explored. In the current study, the fresh porcine muscles are imaged at room temperature with a wide-field MM imaging polarimeter over 26 hours to visualize dynamics of tissue optical properties through applying Lu-Chipman decomposition. The frequency distribution histograms (FDHs) and statistical analysis of the MM elements show prominent changes over time. The wavelength spectra of both total depolarization and scalar retardance have dips at 550 nm whereas their values continuously increase with time; the former is referred to the increase of number of scattering events and decrease of myoglobin absorption in the red part of visible spectra related to meat color and freshness, while the latter is associated with the increase in birefringence and meat tenderness. The obtained results are promising to develop a novel fast non-contact optical technique for monitoring of meat quality.

KEYWORDS
polarized light, Mueller matrix, meat, freshness, depolarization, statistical analysis

1 | INTRODUCTION

In recent years, the studies on interaction of polarized light with biological tissues have shown promising results in the various biomedical applications [1]. The biological tissues usually consist of a huge variety of microstructures and functional units. It is known that the cell dimensions are larger than the wavelength of the visible and near-infrared (NIR) range for a post-mortem tissue [2]. Therefore, tissue cells create inhomogeneities and optical anisotropy leading to dominant Mie scattering of transmitted or backscattered polarized light. The changes of polarization state of the incident light due to multiple scattering within an optically thick biological tissue sample [3] may provide information about the level of victuals freshness [4–6].

The multiple scattering of polarized light within optically thick tissue sample will be affected by the tissue either living or post-mortem. For meat, as a post-mortem tissue, dynamic temporal changes are observed as a result of ongoing chemical processes and shape deformation due to water evaporation at both intracellular and extracellular levels. Polarization measurement techniques detect the changes in polarization state of the reflected or transmitted light signal after its interaction with a sample. When probing meat with polarized light, depolarization and rotation of the orientation of the polarization plane are dependent on the preferential orientation of the elongated muscle cells and meat aging [7,8]. Although there have been studies on meat freshness applying spectroscopic approaches [9], the multiple scattering at visible and near-infrared wavelengths causes difficulties for quantitative tissue spectroscopy and imaging because of shallow penetration depth and the inhomogeneity of tissue which obscures the desired image information [10]. Hence, there is a growing interest to apply polarimetric imaging techniques for investigation of biomedical tissues due to the fact that diffusely scattered light is often partially polarized to an extent, which can be experimentally detected and carry additional non-redundant information on tissue optical properties [11–13].

During propagation of light through a scattering medium, the polarization state of light may alter not only due to the scattering, but also because of the anisotropy of refractive index (birefringence) and anisotropy of absorption (diattenuation) in the medium [7]. The propagation of polarized light through such randomly inhomogeneous medium will cause partial or full depolarization, which depends on tissue microstructure and the wavelength of incident light [14]. Since most of the meat components such as fibrils and connective tissue fibers have a precise longitudinal arrangement of the proteins, they will cause tissue birefringence [15].

Although Mueller matrix imaging polarimetry (MMIP) provides rich qualitative information of optical properties of biological tissues, applying this polarimetric based technique for investigating raw meat quality over time has not yet been explored yet, especially in a view of using it as novel technique for the food quality control in food industry. In this paper, we present the results of our studies with MMIP technique of temporal evolution of scattering and anisotropic properties of fresh meat related to the changes in its sarcomeres and myofibrillar structures over time.

1.1 | Meat structure

Degradation of meat proteins is one of the main consequences of freshness decay during its storage [16]. Meat proteins are classified into three different groups: sarcoplasmic (water-soluble proteins such as myoglobin and haemoglobin), myofibrillar (salt-soluble proteins including myosin and actin), and connective tissue (insoluble proteins) such as collagen and elastin [17]. Forming a large proportion of muscle tissues, myofibrils are periodical sarcomeres with distinct anisotropic refractive index, causing birefringence and scattering in a muscle tissue [18]. In addition, holding the most of water in a muscle cell [19], myofibrils play an important role in meat quality assessment to determine the texture and water holding capacity [20].

Meat color and tenderness are two key factors to evaluate meat freshness whereas the former one is mainly attributed to the amount of myoglobin [21,22] as a sarcoplasmic protein. The latter has been determined by the binding interaction of connective tissue (collagen) and myofibrillar structures (myosin and actin) during the conversion of muscle to meat through physical and biochemical changes [20]. Previous studies on beef muscle samples have shown that samples with short sarcomeres and smaller concentration of myoglobin tend to have higher degree of scattering and birefringence leading to higher paleness and lower tenderness of the meat [15]. In our studies, we investigated the changes of the myofibrils and sarcomeres structures of a porcine muscle sample over time by using polarized light for extracting the helpful information of meat quality. The depolarization is related to the scattering properties of the tissue, retardance and diattenuation enable one to quantify different types of meat anisotropy, mainly its birefringence due to the presence of collagen fibers or myofibrils (myosin structures) [23].

1.2 | Mueller matrix polarimetry

Polarimetric imaging methods have several advantages over other traditional optical imaging techniques such as higher image contrast and providing a unique prospect to reveal additional information that cannot be resolved by other optical imaging modalities [12,23–25]. Among different polarimetric techniques, MM polarimetry is the one which can provide a complete characterization of the polarimetric properties (including diattenuation, dichroism, and depolarization) in addition to microstructural and optical information of a scattering media such as biological tissues [26–29]. Therefore, MMIP is becoming increasingly attractive for distinguishing the structural features of biological tissue in food quality control and medical diagnostics [18,24,28,30–37].

Optical characterization of biological tissue within the framework of the Stokes-Mueller formalism is based on measuring the bulk tissue's polarimetric transfer function, known as its Mueller matrix. This information-rich tissue signature includes the full polarization information reflecting its biophysical properties [38]. MM is a 4×4 matrix with real valued coefficients that transforms a 4×1 Stokes vector representing a polarization state of light impinging on the sample into another 4×1 Stokes vector representing a polarization state of light emerging after the interaction with a sample [39,40],

$$S_{out} = M \cdot S_{in} = \begin{bmatrix} M_{11} & M_{12} & M_{13} & M_{14} \\ M_{21} & M_{22} & M_{23} & M_{24} \\ M_{31} & M_{32} & M_{33} & M_{34} \\ M_{41} & M_{42} & M_{43} & M_{44} \end{bmatrix} \cdot S_{in} , \qquad (1)$$

where S_{in} and S_{out} are the Stokes vectors of incident and outgoing light beams respectively, M is the sample Mueller matrix that contains all information about optical properties [41,42]. The Stokes vector is given by:

$$S = \begin{bmatrix} I \\ I_x - I_y \\ I_{+45} - I_{-45} \\ I_{LC} - I_{RC} \end{bmatrix} = \begin{bmatrix} I \\ Q \\ U \\ V \end{bmatrix} , \qquad (2)$$

where I is the total light intensity and I_x, I_y, I_{+45}, I_{-45} ; I_{LC} ,I_{RC} are the intensities measured through a linear polarizer with the transmission axis oriented along the *x*, *y*, +45° and -45° directions of the laboratory coordinate system, respectively, or through left (LC) or right (RC) circular polarizer [43].

Wide field MMIP measures the spatially dependent polarization properties of samples in the form of MM images. The polarization state generator (PSG) produces polarization states of the light beam incident on the object under study. The reflected / transmitted light goes through the polarization state analyzer (PSA) before being detected. In general, at least 16 intensity measurements have to be performed in order to determine the MM of a sample [44].

All of the MM elements were normalized by M_{11} which will produce dimensionless quantities varying from -1 to 1. Different decomposition techniques have been developed to extract the information on polarization properties of the sample encoded in all 16 elements of the MM, e. g. Mueller matrix polar decomposition (MMPD) [45] and the Mueller matrix transformation (MMT) [32,46]. Here, we applied Lu-Chipman decomposition [45] which shows any physically realizable MM [47] can be decomposed into a product of three MMs of the basic optical components including diattenuator (D), followed by retarder (R), and depolarizer (Δ) [45]. Biological tissues are highly scattering media composed of cells, protein fibers and optically active molecules, so they are expected to possess such polarimetric properties as depolarization, linear birefringence, and optical activity [48]. Each of these tissue properties can be obtained separately when using the MMPD (applied pixelwise in case of MMIP):

$$M = M_\Delta M_R M_D , \qquad (3)$$

where M_Δ, M_R, M_D are the matrices of a depolarizer, a retarder and a diattenuator, respectively [36].

Here, we have applied MMIP approach to investigate changes in optical properties of fresh meat with time, including total depolarization, and scalar retardance.

2 | MATERIALS AND METHODS

2.1 | Experimental setup

In this study, we used a custom-built multi-wavelength wide-field MMIP system, which has been developed and installed in the Laboratory of Physics of Interfaces and Thin Films, Ecole Polytechnique (LPICM), Palaiseau, France. An optical scheme of the setup is shown in Figure 1A including a spectral filter zoom system, a CCD camera and a halogen lamp as the source of illumination. A Polarization State Generator (PSG) consisting of a linear polarizer and two ferroelectric liquid crystals (FLCs) were used for the generation of polarized light. Each LC works essentially as a wave plate with the fixed retardation whose fast axis orientation switches between θ and θ+45 degrees. The initial orientation of the fast axes of two LCs was fixed at the angles θ_1 and θ_2, respectively. To analyze the backscattered light, a Polarization State Analyzer (PSA) consisting of the same elements, but assembled in a reverse order, was used in the detection arm. The detailed description of the instrument can be found elsewhere [49].

This MMIP system operates in a visible wavelength range (450-700 nm) and enables complete polarimetric characterization of biological tissue by measuring the wide-field (up to 5×5 cm^2) MM images of the sample.

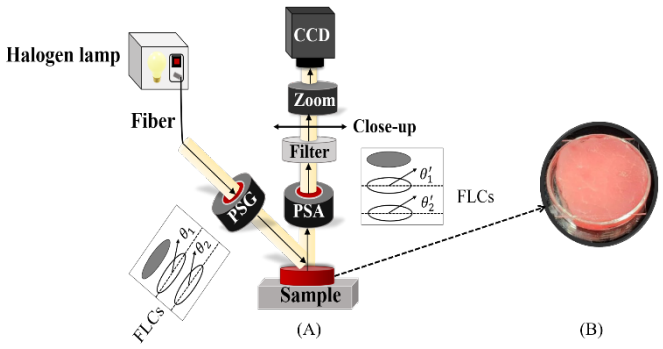

FIGURE 1 (A) Schematic presentation of the MMIP used in the study; (B) Photograph of a sample (porcine muscle). A glass slide was placed on top of the sample to flatten the surface.

The PSG generates four different states of polarization of incident light beam, that interacts with a sample and then is projected sequentially on four polarization states of PSA, which are identical to those of the PSG. Hence, sixteen measurements are performed to obtain the complete MM images of the tissue sample. The measurements were repeated (typically 5-10 times) for each state of polarization and averaging over the acquired images was performed in order to achieve the satisfactory signal-to-noise ratio. The acquisition time of a complete set of sixteen averaged raw intensity images was typically a few seconds for each measurement wavelength. Then, MM images of the sample were obtained from the measured set of sixteen raw intensity images by using the calibration data (measurements of reference samples) and applying a set of linear algebra operations. Polarimetric images of the fresh porcine muscle samples were taken at multiple wavelengths: 450, 500, 550, 600, 650, and 700 nm.

We have used 10 samples from fresh porcine muscle bought from a local supermarket. The samples of about 1 cm thickness were cut into 3×3 cm^2 pieces, then placed in a glass container and covered with a glass slide in order to reduce specular reflection from uneven surface of the tissue (Figure 1B). All samples were stored in air at room temperature (23°). They were measured several times a day, with an average interval of two hours, to observe early changes in optical parameters due to the meat aging process.

2.2 | Analysis of MM elements and polarimetric parameters

To interpret the measured MM of the biological tissue and enhance the accuracy, we applied statistical analysis of MM images of the elements, as well as total depolarization, and scalar retardance obtained by using MMPD of measured MM. This approach has been also applied in previous studies [34,50,51].

The MM data can be presented in the form of two-dimensional *(m×n)* distributions of matrix elements, known also as Muller matrix images and indicated here as *M(m×n).* For the quantitative evaluation of two-dimensional distributions *M(m×n)*, a set of the central statistical moments of the first (Z_1; mean value), second (Z_2; variance), third (Z_3; skewness), and fourth (Z_4; kurtosis) orders was used [50,52–55]:

$$Z_1 = \frac{1}{N}\sum_{j=1}^{N} M_j$$

$$Z_2 = \sqrt{\frac{1}{N-1}\sum_{j=1}^{N}(M_j - Z_1)^2}$$

$$Z_3 = \frac{1}{Z_2^3}\frac{1}{N}\sum_{j=1}^{N}(M_j - Z_1)^3 \qquad (4)$$

$$Z_4 = \frac{1}{Z_2^4}\frac{1}{N}\sum_{j=1}^{N}(M_j - Z_1)^4 ,$$

where $N = m \times n$ is the number of pixels of the CCD-camera.

A low value of the variance (Z_2) indicates that the distribution of the measured data would be close to the mean value (Z_1), while a high value of the variance shows that the data points are more spread out around the mean value and from each other. The third and fourth statistical moments Z_3 and Z_4 represent the skewness and kurtosis of the frequency distribution histogram (FDH), respectively. The skewness (Z_3) indicates the asymmetry of the FDH and can be positive or negative. A negative (or positive) skewness value shows that the tail on the left (or the right) side of the FDH is longer (or shorter) than that on the right (or the left) side. The kurtosis (Z_4) characterizes the strength of the outliers of the distribution in FDH [56]. High (low) kurtosis in a dataset demonstrates that data has heavy (light) tails or outliers [54].

The MM elements of isotropic partially depolarizing samples have non-zero elements on the diagonal only, and the absolute values of the M_{22} and M_{33} elements are equal, whereas for partially polarizing anisotropic samples, MM has both diagonal and non-diagonal non-zero elements due to the polarized light scattering and phase shift between its components related to sample anisotropic refractive index or birefringence [18,57]. Smaller values of M_{22} and M_{33} mean larger depolarization [46,58]. Finally, the values of diagonal elements M_{22}, M_{33} and M_{44} are closely related to the depolarization and absorption properties of the samples [18,33] which are our focus of study in the current work.

Here, we first recorded the 2D backscattering MM images of the samples, and then, transformed the pixelated images to FDHs for the statistical analysis. Finally, the central statistical moment method was applied to the FDHs of MM elements, total depolarization and retardance. In addition, we assessed the changes of total depolarization and retardance spectra and their statistical moments changes over time.

3 | RESULTS AND DISCUSSION

The changes in total depolarization and scalar retardance spectra are displayed in Figure 2A and 2B, respectively, for fresh (0 hour; green line) and aged (26 hours; red line) tissue sample. The error bars represent standard deviation of the parameters. A clear difference between two spectra measured at different time can be seen in both figures. The values of total depolarization and retardance are averaged over 800×600 pixels of corresponding images measured at different wavelengths. Apparently, the values of total depolarization and scalar retardance are increasing with the wavelength for both measurement time points, except for the dip at 550-nm wavelength which is attributed to the highest amount of myoglobin absorption [9,59] (Figure 2A). Higher concentration of myoglobin which tend to have lower degree of scattering and birefringence. The detected photons travel shorter distance within the sample compared to long path photons that are absorbed [15,60].

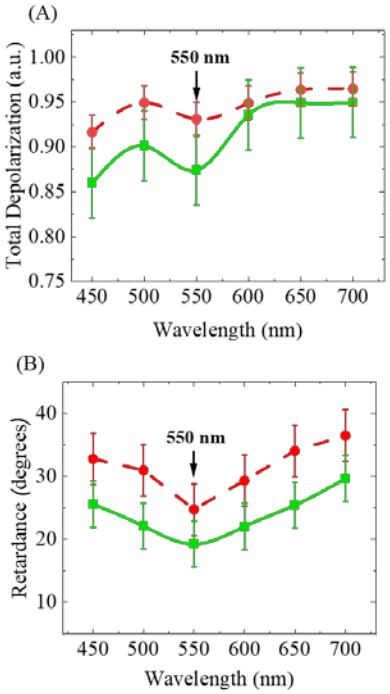

FIGURE 2 Wavelength dependence of (A) total depolarization and (B) scalar retardance for fresh (0 hour; green line) and aged (26 hours; red line) of a porcine muscle sample of 1-cm thickness stored at room temperature (23℃).

Since the polarimetric parameters at 550 nm wavelength have distinctive behavior compared to the rest of spectra (Figure 2A and 2B), we have selected this wavelength for further analysis. Figure 3 demonstrates the images of backscattering 4×4 MM of a porcine muscle tissue (1 cm thick) measured at 550 nm wavelength for fresh (0 hour; Figure 3A) and aged (26 hours; Figure 3B) conditions stored in air at room temperature (23°). According to Figure 3, as the time increases, the diagonal elements of MM change prominently; M_{22} value for aged sample (Figure 3B) is higher than the fresh sample (Figure 3A) while M_{33} and M_{44} obviously decrease after 26 hours which will be contributed to larger depolarization.

The MM elements in both Figures 3A and 3B are non-diagonal proving the anisotropic features of the medium due to the well aligned muscle fibers. However, the values of non-diagonal elements did not exceed 0.025.

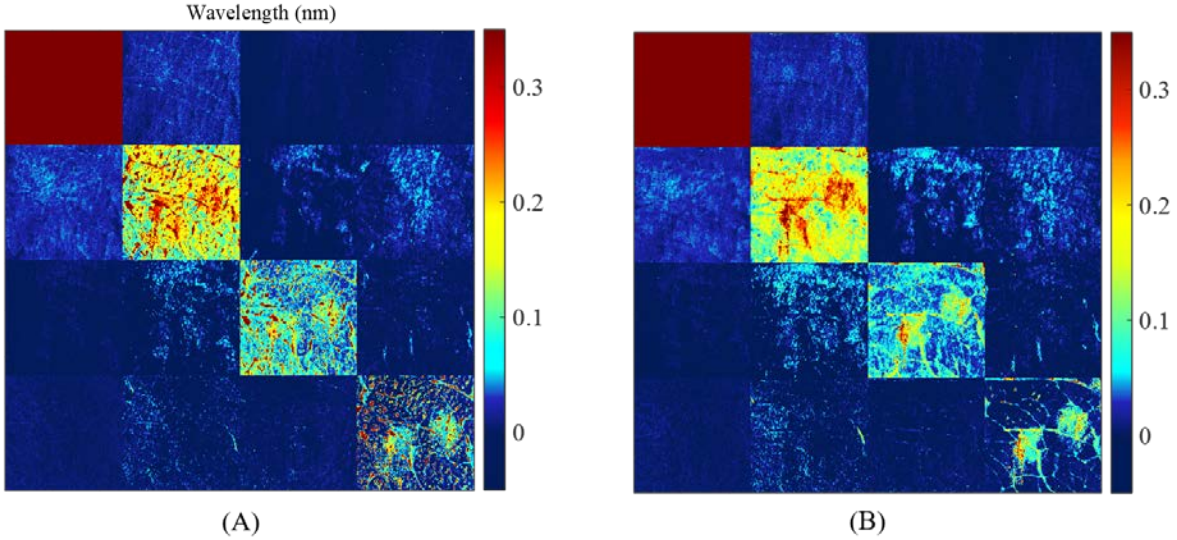

FIGURE 3 Experimental backscattering 4×4 MM images of a porcine muscle sample of 1-cm thickness measured at 550-nm wavelength: (A) fresh (0 hour) and (B) aged (26 hours) stored at room temperature (23℃). The field of view was 2 ×2cm^2 and each element of polarimetric images was normalized by the corresponding pixel value of the M_{11} image.

Although the 2D MM images contain more detailed spatial information on a sample, transforming the images into FDH curves can better reflect some intrinsic structural properties of tissue compared to 2D images of MM elements. Similar to the approach used in [18], Figure 4 shows the normalized FDH diagrams of MM elements of a glass-covered porcine muscle sample measured at 550 nm wavelength for fresh (0 hour; black line) and aged (26 hours; red line) conditions stored in air at room temperature (23°). The horizontal axis of each FDH represents the value of the pixel from the corresponding MM element, while the vertical axis represents the probability distribution.

It can be seen in Figure 4 that FDHs of diagonal elements M_{33} and M_{44} vary with time. Moreover, analyzing different groups of elements can help to find the origin of anisotropy [25]. Here, the FDHs of non-diagonal elements including M_{23}, M_{31}, M_{32}, M_{41} and M_{42} measured after 26 hours are shifted towards larger values showing the increase in the sample anisotropy. However, this variability makes it difficult to decide if the origin of anisotropy is due to the scattering properties of tissue or its birefringence. Furthermore, M_{23}, M_{32} and M_{41} elements demonstrate the most pronounced shift of FDHs towards higher values with time which for the case of M_{23} and M_{32}, it can be referred to the direction of the aligned fibers or the birefringence.

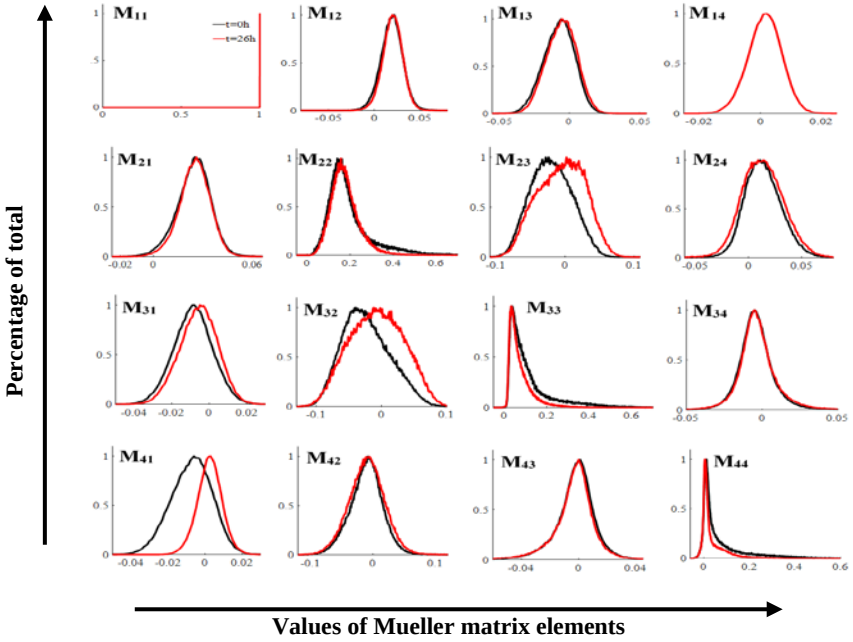

FIGURE 4 Frequency distribution histograms (FDH) of the MM elements of a 1 cm thick porcine muscle sample at fresh (0 hour; black line) and aged (26 hours; red line) state measured at 550 nm light wavelength and stored at room temperature (23°). The areas under the FDH are normalized to 1.

To make the evaluation quantitative, 3D graphs of the statistical moments (Z_i) characterizing distributions of each MM element (normalized to M_{11}) of a porcine muscle sample measured at 550 nm at fresh (0 hour; Figure 5A,C,E,G) and aged (26 hours; Figure 5B,D,F,H) state in air at room temperature are listed in Figure 5. According to Figure 5A, the largest values of mean for the fresh sample (0 hour) belong to M_{22}, M_{23}, M_{24} and M_{44} while for the aged sample (26 hours; Figure 5B), M_{22}, M_{23}, M_{24}, M_{32} and M_{33} have the largest mean values. The values of M_{22} and M_{33} are not equal and their difference is increasing over time which shows the increase in anisotropy of linear depolarization by the sample [54,61] The positive and low mean values of M_{34} and M_{43} elements may be contributed to the weak birefringence effect in this sample. In addition, M_{22} and M_{33} values of Z_1 increase over time while for M_{44}, it decreases considerably.

Meanwhile, the values of variance (Figure 5C and 5D) for most of the elements change slightly over time which indicates distributing width of the FDHs does not change noticeably with time. However, M_{22}, M_{23}, M_{32}, and M_{33} slightly have larger values for both times compared to the other elements. According to Figure 5E and 5F, the skewness values considerably decrease over time. Moreover, the variance values of the central elements (M_{22}, M_{23}, M_{32}, M_{33}) and M_{41} are obviously higher than other elements for both state of freshness.

The kurtosis values (Figure 5G and 5H) of the central elements are smaller compared to the other elements for both measurement times and furthermore, the values of kurtosis slightly decrease over time.

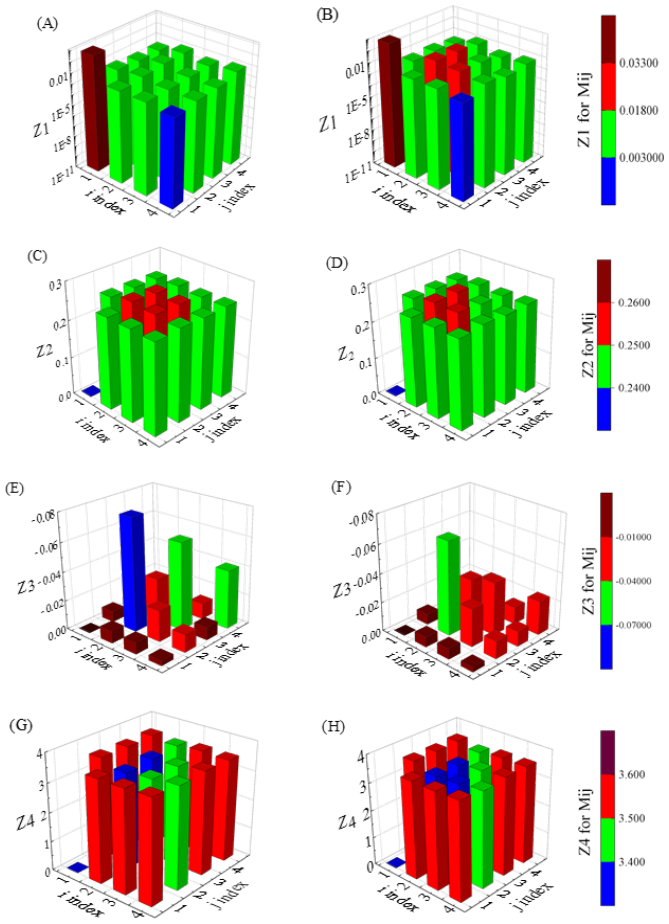

FIGURE 5 Statistical moments (Z_i) of the (A and B) first (Z_1; mean value), (C and D) second (Z_2; variance), (E and F) third (Z_3; skewness), and (G and H) fourth (Z_4; kurtosis) orders (normalized to M_{11}) characterizing the distributions of the MM elements of a porcine muscle sample measured at 550 nm for fresh (0 hour; A,C,E,G) and aged (26 hours; B,D,F,H) in air at room temperature (23°).

Figures 6 and 7 display total depolarization ($\Delta(x,y)$) (Figure 6A-6C) and retardance ($R(x,y)$) (Figure 6D-6F) images obtained by MMPD applied pixel-wise to the measured MM and the corresponding histograms ($N(\Delta)$) of total depolarization (Figure 7A-7C) and retardance (Figure 7D-7F) of a porcine muscle sample of 1 cm thickness measured at 550 nm wavelength fresh (Figures 6 and 7; panel A and D) after 6 hours , (Figures 6 and 7; panel B and E) and aged (26 hours) (Figures 6 and 7; panel C and F) in air at room temperature (23°). Apparently, depolarization is very strong (~0.9) and there are prominent differences between the images over time (Figure 6A-6C) showing some specific regions of the sample evolve differently over time. The strong depolarization observed in some regions at all three measurement time points could be explained by the presence of a well-ordered myofibrils (most probably myosin which has thicker myofibrillar structure). Since there is no noticeable shift in the histograms over time (Figure 6B; panels 1-3), the asymmetry of the distribution related to the skewness value (Z_3) must have been kept. Meanwhile, the tail heaviness of the histograms attributed to kurtosis (Z_4) of total depolarization is increasing over time which will need further studies to analyze.

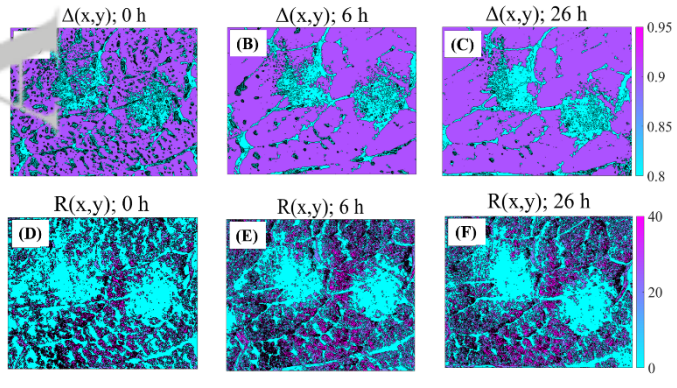

FIGURE 6 Images of the total depolarization ($\Delta(x,y)$; A-C) and scalar retardance ($R(x,y)$; D-F) of a porcine muscle sample of 1 cm thickness measured at 550 nm wavelength after 0 hours (A and D), 6 hours (B and E) and 26 hours (C and F) in air at room temperature (23°).

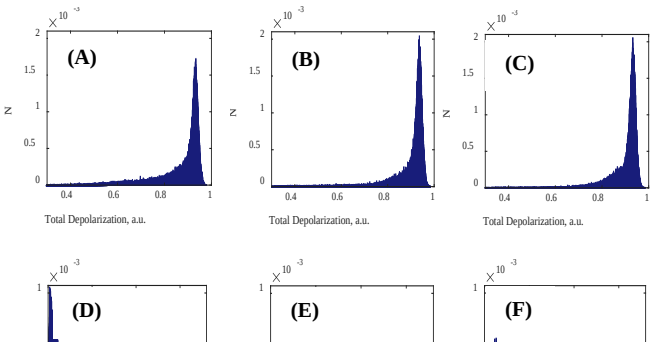

FIGURE 7 Histograms (N) of the total depolarization ($\Delta(x,y)$; A-C) and scalar retardance ($R(x,y)$; D-F) of a porcine muscle sample of 1 cm thickness measured at 550 nm wavelength after 0 hours (A and D), 6 hours (B and E) and 26 hours (C and F) in air at room temperature (23°).

To have a deeper view of the changes happening during the meat aging process and as a quantitatively description, time dependency of the statistical moments of total depolarization and scalar retardance FDHs has been analyzed after curve fitting in Figure 8 at 550-nm wavelength through applying Equation 4 and replacing M with Δ (total depolarization) and R(scalar retardance) values. Clearly, the mean values of both total depolarization and scalar retardance (Figure 8A and 8B; Z_1) increase smoothly with time that can be explained by the increasing of the number of scattering events over time [59,62] due to water evaporation and increasing spaces between muscle fiber bundles [63].

According to Figure 8A (Z_2), the variance values of total depolarization decrease over time showing the data points are distributed closer to the mean value whereas for scalar retardance (Figure 8B; Z_2), the data are distributed more spread around the mean value (Z_1). Figure 8A (Z_3) shows that the distribution of total depolarization values is negatively skewed (wider left FDH tail towards lower values; Figure 7A-7C) while for scalar retardance (Figure 8B), they are positive indicating that the right FDH tail is wider and it is extended towards higher values (Figure 7D-7F). For both total depolarization and scalar retardance values, skewness noticeably decreases after 26 hours. Furthermore, kurtosis values for total depolarization increase with time (Figure 8A; Z_4) while for scalar retardance (Figure 8B; Z_4), kurtosis declines over time contributed to the tail heaviness direction of the distribution.

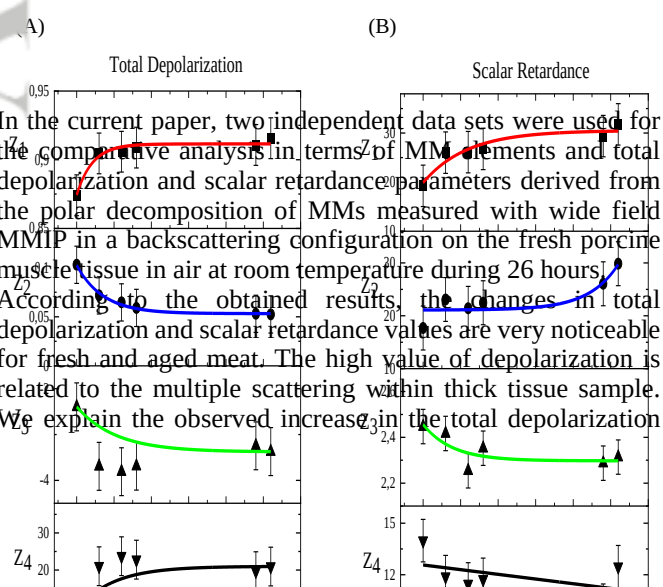

FIGURE 8 Images of statistical moments (Z_i) for (A) total depolarization and (B) scalar retardance of a porcine muscle sample of 1 cm thickness measured at 550 nm wavelength over 26 hours in air at room temperature (23°). Solid lines show exponential fitting functions and error bars represent standard deviation of statistical moments.

Here, we can see that the increase of total depolarization is most probably caused by the increase in the number of scattering events. Furthermore, the increase of scalar retardance over time may be contributed to water evaporation leading to myosin bundles densification and alignment which can increase the anisotropy of the refractive index including sample birefringence.

These preliminary studies indicate that the FDHs and its statistical moments demonstrated the potential to give a quantitative metrics to assess meat quality with time.

4 | CONCLUSION

In the current paper, two independent data sets were used for the comparative analysis in terms of MM elements and total depolarization and scalar retardance parameters derived from the polar decomposition of MMs measured with wide field MMIP in a backscattering configuration on the fresh porcine muscle tissue in air at room temperature during 26 hours. According to the obtained results, the changes in total depolarization and scalar retardance values are very noticeable for fresh and aged meat. The high value of depolarization is related to the multiple scattering within thick tissue sample. We explain the observed increase in the total depolarization with wavelength by the decrease of light absorption by myoglobin in red part of the visible light spectrum, which, in turn, leads to the increase of the average number of scattering events for the detected photons. On the other hand, the least value of depolarization at the 550 nm wavelength could be arguably explained by the highest absorption of myoglobin, which is responsible for meat color and freshness. Therefore, the increasing slope of the total depolarization mean values changes with time at the 550-nm wavelength could be referred to the decrease in myoglobin absorption over time and disordering of the fibrillary structure of the samples. These

changes in depolarization of fresh and aged meat samples are clearly detected in polarimetric images and time-dependent graphs and could provide a quantitative metrics for a non-invasive assessment of meat freshness.

Although more studies are still needed to reveal the relationships between tissue morphology and the statistical moments of FDHs of MM elements, we found some tendencies by analysis of statistical moment elements changes over time. The results discussed above suggest that (1) the shapes of FDHs (values of Z_2, Z_3, and Z_4) are partially sensitive to aging in meat freshness level and they will change over time; (2) The FDHs and corresponding statistical moment parameters of MM elements are good quantitative indicators of the microstructures changes over time.

However, further studies will be needed to examine this technique applied on the samples prepared immediately from the slaughtered animal to compare the features of "fresh" condition with the performed measurements with the samples from the market packages. Other types of meat product including chicken, beef or fish have been considered to be investigated as the prospective plans. In addition, the effect of oxygenation and water evaporation will be considered more deeply including investigation of the effect of rehydration.

ACKNOWLEDGMENTS

This work received funding from the European Union's Horizon 2020 research and innovation program under the Marie Sklodowska-Curie (grant agreement No 713606); Cost Actions (CA16118); Academy of Finland (grant (314369, 325 97), the ATTRACT project funded by the EC under Grant Agreement 777222; MEPhI Academic Excellence Project (Contract No. 02.a03.21.0005, IM), National Research Tomsk State University Academic D.I. Mendeleev Fund Program, Campus France PHC Dumont D'Urville project POLANNs (No. 43261UE), INFOTECH strategic funding and Russian Science Foundation (Project19-72-30012).

AUTHOR CONTRIBUTIONS

M.P. performed the experiments, data analysis and wrote the manuscript. A.P. was involved in the study design, manuscript review and editing. A.B. provided guidance in manuscript finalization. A.P. taught M.P. to work with MMIP system. T.N. helped with the study design, data analysis, manuscript writing and editing. I.M. developed the concept and study design, managed the project, reviewed and edited the manuscript.

CONFLICT OF INTEREST

The authors declare no financial or commercial conflict of interest.

REFERENCES

[1] T. Novikova, I. Meglinski, J. C. Ramella-Roman, V.V. Tuchin, *J. Biomed. Opt.* **2016**, 21(7), 071001.

[2] G. Zaccanti, D. Contini, in: *Photon migration and imaging of biological tissues* (Ed: A. Consortini), Trends in Optics: Research, Developments and Applications, Academic Press, San Diego, **1996**, chap. 3.

[3] S. D. Gupta, N. Ghosh, A. Banerjee, in: *Wave Optics: Basic Concepts and Contemporary Trends*, CRC Press, Boca Raton, **2015**.

[4] P. Tománek, J. Mikláš, H. M. Abubaker, L. Grmela, in: *Proc. AIP Conf. 1288*, Delphi **2010**, 127.

[5] H. M. Abubaker, P. Tománek, L. Grmela, in: *Proc. SPIE 8073*, Prague **2011**, 80730U.

[6] M. Sarkar, N. Gupta, M. Assaad, *Appl. Opt.* **2019**, 58(23), 6396.

[7] A. A. Blokhina, V. A. Ryzhova, V. V. Korotaev, M. A. Kleshchenok, in: *Proc. SPIE 10239*, Prague, **2017**, 102390K.

[8] H. M. Abubaker, *PhD thesis*, Brno University of Technology (Czech Republic), **2013**.

[9] M. Peyvasteh, A. Popov, A. Bykov, I. Meglinski, *J. Phys. Commun.* **2020**, 4(9), 95011.

[10] S. Yoon, M. Kim, M. Jang, Y. Choi, W. Choi, S. Kang, W. Choi, *Nat. Rev. Phys.* **2020**, 2, 141.

[11] K. C. Hadley, A. Vitkin, *J. Biomed. Opt.* **2002**, 7(3), 291.

[12] A. Pierangelo, S. Manhas, A. Benali, M. R. Antonelli, T. Novikova, P. Validire, B. Gayet, A. De Martino, in: *Proc. SPIE 7895*, San Frncisco, **2011**, 78950E.

[13] M. Kupinski, M. Boffety, F. Goudail, R. Ossikovski, A. Pierangelo, J. Rehbinder, J. Vizet, T. Novikova, *Biomed. Opt. Express*. **2018**, 9(11), 5691.

[14] A. A. Blokhina, V. A. Ryzhova, M. A. Kleshchenok, A. Y. Lobanova, in: *Proc. SPIE 103331*, Munich, **2017**, 103331F.

[15] H. J. Swatland, University of Guelph (Canada), **2012**.

[16] D. Dave, A. E. Ghaly, *Am. J. Agric. Biol. Sci.* **2011**, 6(4), 486.

[17] M. Lund, *PhD thesis*, University of Copenhagen, **2007**.

[18] H. He, C. He, J. Chang, D. Lv, J. Wu, C. Duan, Q. Zhou, N. Zeng, Y. He, H. Ma, *J. Biophotonics* **2017**, 10(5), 664.

[19] E. Huff-Lonergan, S. M. Lonergan, *Meat Sci.* **2005**, 71(1), 194.

[20] S. Fowler, *PhD thesis*, Charles Sturt University (Australia), **2015**.

[21] K. Chao, Y. Liu, Y. R. Chen, D. W. Thayer, W. R. Hruschka, *Am. Soc. Agric. Eng.* **2002**, 18(6), 745.

[22] S. P. Suman, P. Joseph, *Annu. Rev. Food Sci. Technol.* **2013**, 4(1),

79.

[23] N. G. Khlebtsov, I. L. Maksimova, I. Meglinski, L. V. Wang, V.V. Tuchin, in: *Handbook of Optical Biomedical Diagnostics* (Ed: V.V. Tuchin), SPIE Press, Bellingham, **2016**, chap. 1.

[24] J. Qi, D. S. Elson, *J. Biophotonics* **2017**, 10(8), 950.

[25] K. U. Spandana, K. K. Mahato, N. Mazumder, *Lasers Med. Sci.* **2019**, 34(7), 1283.

[26] S. L. Jacques, J. C. Ramella-Roman, K. Lee, *J. Biomed. Opt.* **2002**, 7(3), 329.

[27] E. Du, H. He, N. Zeng, C. Liu, Y. Guo, R. Liao, M. Sun, Y. He, H. Ma, *J. Innov. Opt. Health Sci.* **2013**, 7(1), 1.

[28] A. De Martino, E. Garcia-Caurel, B. Laude, B. Drévillon, *Thin Solid Films* **2004**, 455–456, 112.

[29] V. V. Tuchin, *Handbook of Coherent-Domain Optical Methods: Biomedical Diagnostics, environmental Monitoring, and Materials Science*, Springer-Verlag, New York, **2013**.

[30] M. Peyvasteh, L. Tryfonyuk,V. Ushenko, A. Dubolazov, O. Vanchulyak, A. Ushenko, Y. Ushenko, M. Gorsky, M. Sidor, Y. Tomka, I. Soltys, A. Bykov, I. Meglinski, *Laser Phys. Lett.* **2020**, 17(11), 9.

[31] A. Pierangelo, A. Nazac, A. Benali, P. Validire, H. Cohen, T. Novikova, B. H. Ibrahim, S. Manhas, C. Fallet, M. R. Antonelli, A. De Martino, *Opt. Express* **2013**, 21(12), 14120.

[32] W. Sheng, W. Li, J. Qi, T. Liu, H. He, Y. Dong, S. Liu, J. Wu, D. S. Elson, H. Ma, *Photonics* **2019**, 6(1), 1.

[33] T. Liu, T. Sun, H. He, S. Liu, Y. Dong, J. Wu, H. Ma, *Biomed. Opt. Express*, **2018**, 9(9), 4413.

[34] M. Borovkova, M. Peyvasteh, O. Dubolazov, Y. Ushenko, V. Ushenko, A. Bykov, S. Deby, J. Rehbinder, T. Novikova, I. Meglinski, *J. Eur. Opt. Soc.* **2018**, 14(1), 4.

[35] J. Zhou, H. He, Y. Wang, H. Ma, in: *Proc. SPIE 10059*, San Francisco, **2017**, 1005926.

[36] S. Forward, A. Gribble, S. Alali, A. A. Lindenmaier, A. Vitkin, *Sci. Rep.* **2017**, 7(1), 1.

[37] K. Rajkumar, P. Sunethri, P. V. K. Rao, V. Padmaja, in: *Proc. ICIC*, Pune, **2015**, 1540.

[38] S. Alali, A. Vitkin, *J. Biomed. Opt.* **2015**, 20(6), 061104.

[39] R. M. A. Azzam, N. M. Bashara, *Ellipsometry and Polarized Light*, Oxford, North-Holland, **1977**.

[40] M. Borovkova, A. Bykov, A. Popov, I. Meglinski, *J. Biomed. Opt.* **2020**, 25(5), 057001.

[41] A. Vitkin, N. Ghosh, A. de Martino, in: *Photonics: Scientific Foundations, Technology and Applications* (Ed: D. L. Andrews), John Wiley & Sons, Inc., **2015**, 4, Chap. 7, p. 239.

[42] A. Mendoza-Galván, E. Muñoz-Pineda, S. J. L. Ribeiro, M. V. Santos, K. Järrendahl, H. Arwin, *J. Opt.* **2018**, 20(2), 024001.

[43] R. A. Chipman, W. S. T. Lam, G. Young, *Polarized Light and Optical Systems*, CRC Press, **2018**.

[44] R. A. Chipman, E. A. Sornsin, J. L. Pezzaniti, in: *Proc. ISPAADT*, Yokohama, **1996**, 2873, 5.

[45] S. Y. Lu, R. A. Chipman, *J. Opt. Soc. Am. A*, **1996**, 13(5), 1106.

[46] C. He, H. He, J. Chang, Y. Dong, S. Liu, N. Zeng, Y. He, H. Ma, *Biomed. Opt. Express*, **2015**, 6(8), 2934.

[47] J. Gil, R. Ossikovski, *Polarized Light and the Mueller Matrix Approach*, CRC Press, Boca Raton, **2016**.

[48] S. J. Matcher, in: *Handbook of Optical Biomedical Diagnostics* (Ed: V. V. Tuchin), SPIE Press, **2016**, Chap. 9, p. 1410.

[49] T. Novikova, J. Rehbinder, S. Deby, H. Haddad, J. Vizet, A. Pierangelo, P. Validire, A. Benali, B. Gayet, B. Teig, A. Nazac, B. Drévillon, F. Moreau, A. De Martino, in: *Proc. Biomed. Opt.* Florida, **2016**, TTh3B.2.

[50] M. Peyvasteh, A. Dubolazov, A. Popov, A. Ushenko, Y. A. Ushenko, I. Meglinski, *J. Phys. D. Appl. Phys.* **2020**, 53(2020), 395401.

[51] M. Borovkova, A. Bykov, A. Popov, A. Pierangelo, T. Novikova, J. Pahnke, I. Meglinski, *Biomed. Opt. Express* **2020**, 11, 4509.

[52] O. Angelsky, A. Ushenko, Y. Ushenko, V. Pishak, A. Peresunko, in: *Handbook of Photonics for Biomedical Science, Series in Medical Physics and Biomedical Engineering* (Ed: V. Tuchin), CRC Press, **2010**, p. 283.

[53] Y. A. Ushenko, *Opt. Spectrosc+*. **2015**, 118(6), 1007.

[54] C. He, H. He, X. Li, J. Chang, Y. Wang, S. Liu, N. Zeng, Y. He, and H. Ma, *J. Biomed. Opt.* **2015**, 20(10), 105009.

[55] V. T. Bachinskyi, O. Y. Wanchulyak, A. G. Ushenko, Y. A. Ushenko, A. V. Dubolazov, I. Meglinski, *Polarization Correlometry of Scattering Biological Tissues and Fluids*, Springer Singapore, **2020**, p. 1.

[56] P. H. Westfall, *Am. Stat.* **2014**, 68, 191.

[57] T. Novikova, A. Pierangelo, S. Manhas, A. Benali, P. Validire, B.

Gayet, A. De Martino, *Appl. Phys. Lett.* **2013**, 102(24), 241103.

[58] M. Sun, H. He, N. Zeng, E. Du, Y. Guo, C. Peng, Y. He, and H. Ma, *Appl. Opt.* **2014**, 53(14), 2949.

[59] B. Kunnen, C. Macdonald, A. Doronin, S. Jacques, M. Eccles, I. Meglinski, *J. Biophotonics* **2015**, 8, 317–23.

[60] G. Lindahl, *PhD thesis*, Swedish University of Agricultural Sciences (Sweden), **2005**.

[61] P. Li, H. R. Lee, S Chandel, C. Lotz, F. K. Groeber-Becker, S. Dembski, R. Ossikovski, H. Ma, T Novikova, *J. Biomed. Opt.* **2020,** 25(1), 015002.

[62] A. Pierangelo, S. Manhas, A. Benali, C. Fallet, J-L Totobenazara, M-R Antonelli, T. Novikova, B. Gayet, A. De Martino, P. Validire, *J. Biomed. Opt.* **2013**, 18, 046014.

[63] J. M. Hughes, M. F. Clarke, P. P. Purslow, R. D. Warner, *Compr. Rev. Food Sci. Food Saf.* **2020** 19, 44.

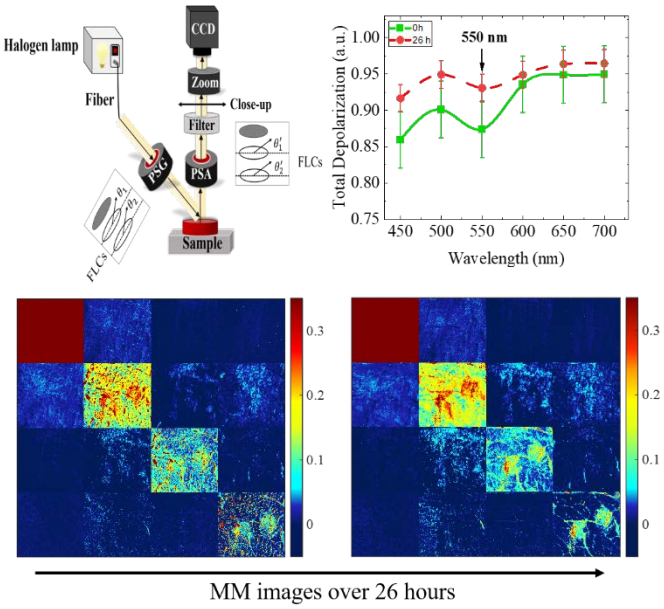

Graphical Abstract for Table of Contents

Here, dynamics of the porcine tissue optical properties over time have been visualized through using Mueller matrix imaging polarimetry. Total depolarization and retardance spectra have dips at 550 nm referred to myoglobin absorption drop (and meat color changes) and increase in birefringence and roughness, respectively. Furthermore, statistical moments analysis of FDHs demonstrates the potential to give a quantitative metrics to assess meat quality with time. The results are promising for a novel approach for monitoring meat quality.

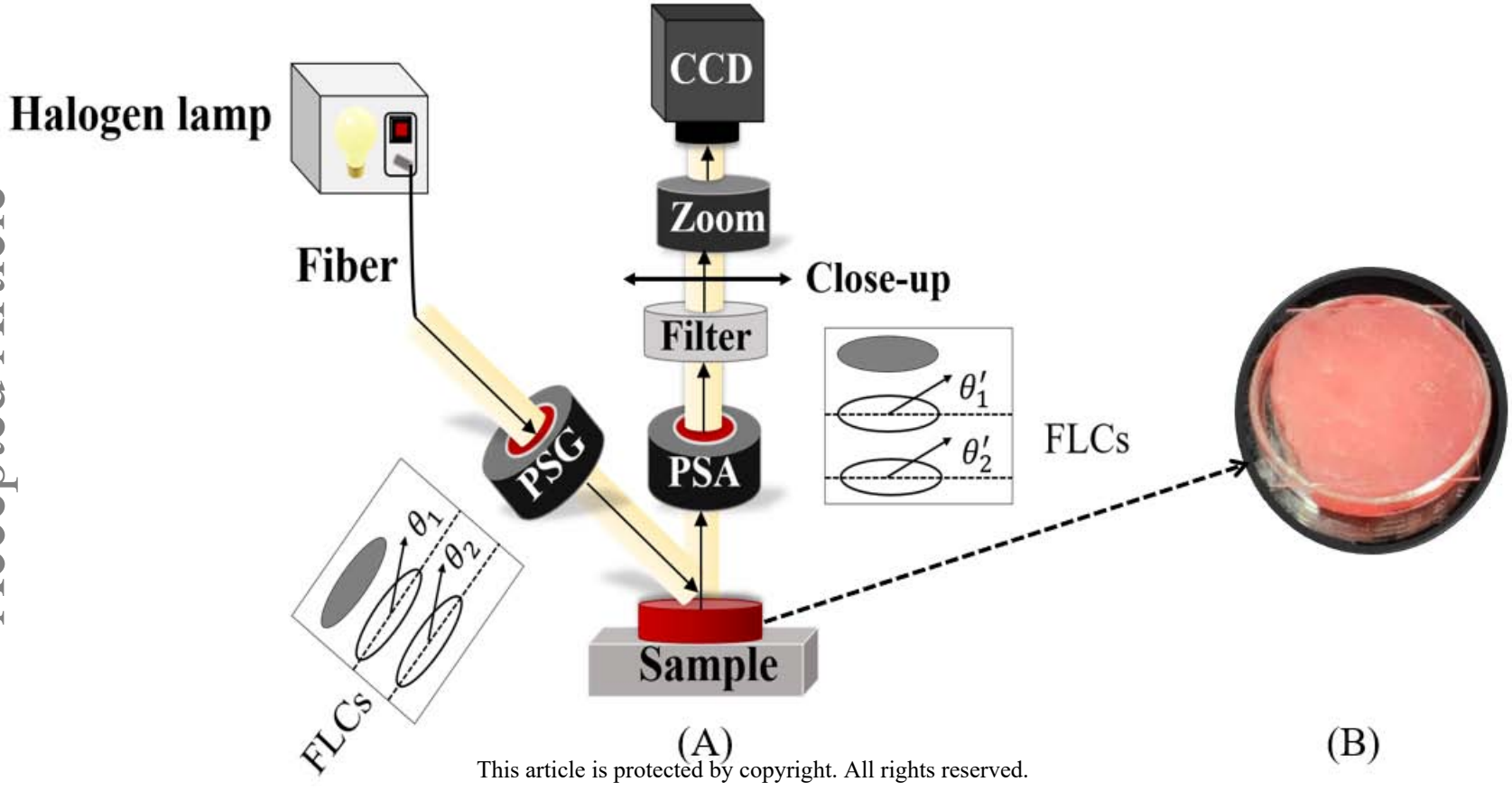

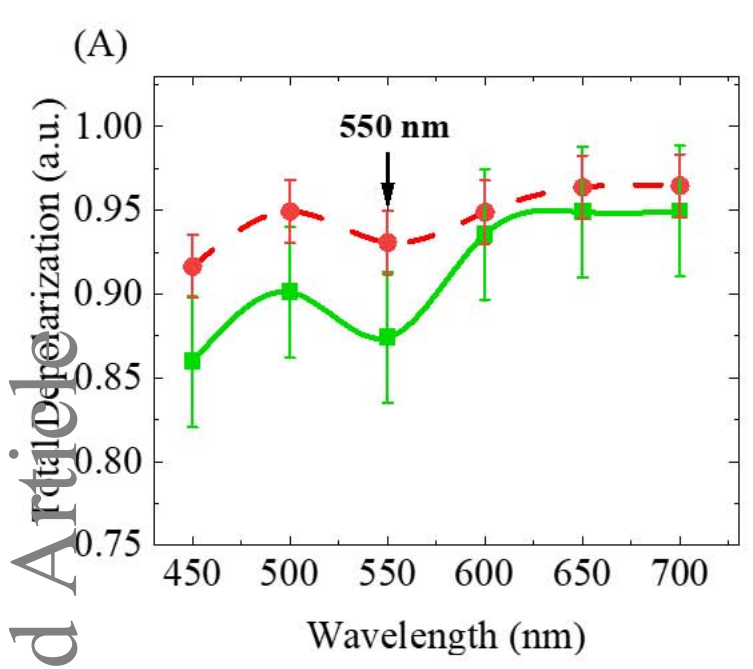

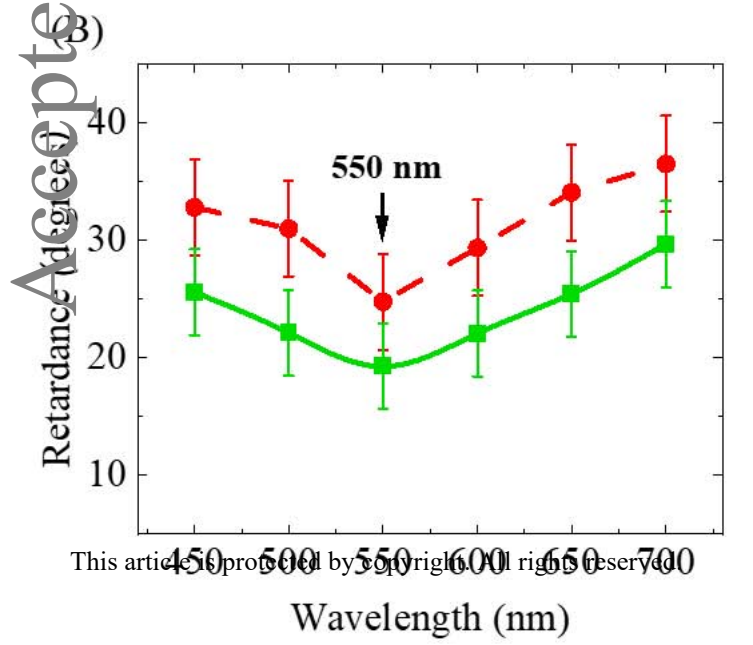

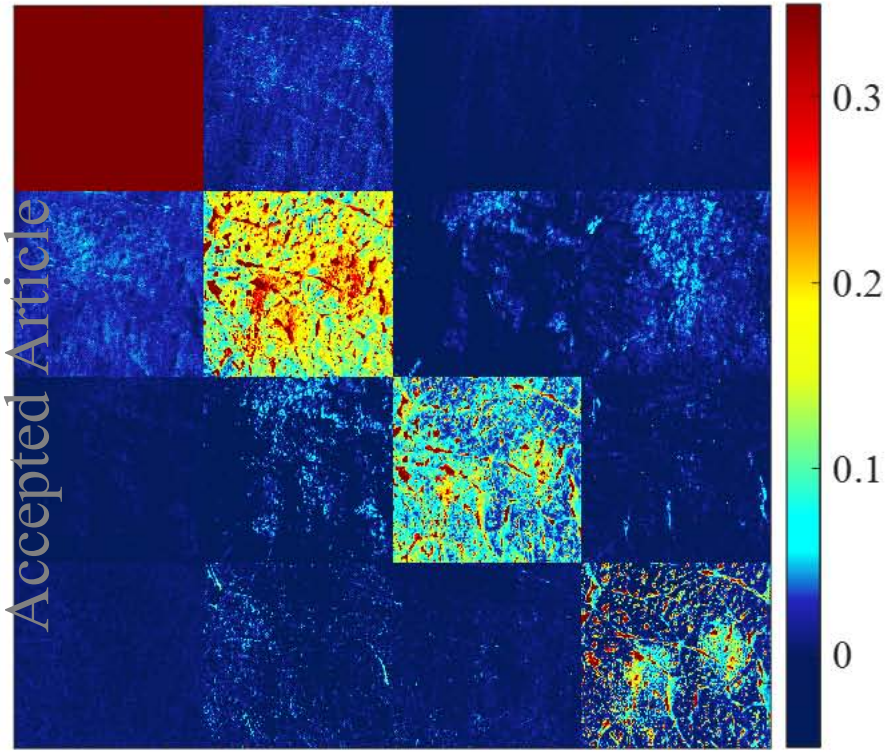

(A)

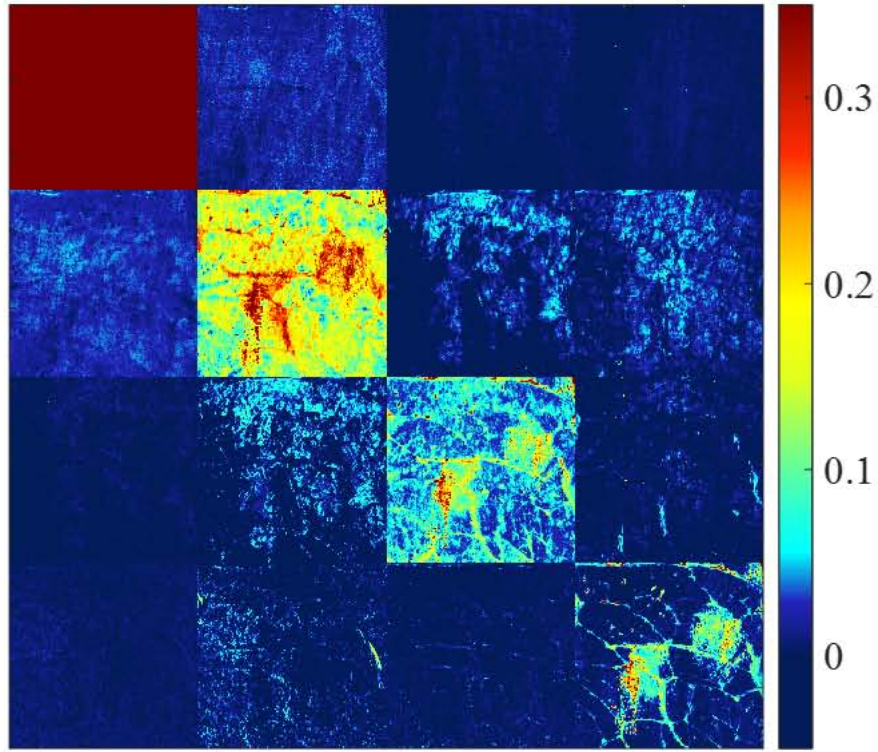

(B)